Nuclear Physics **A365** (1981) 127–141


# BAND CROSSING AND THE PREALIGNMENT $B$(E2) ANOMALY IN $^{126}$Ba

J. P. DRAAYER †, C. S. HAN †† and K. J. WEEKS

*Department of Physics and Astronomy, Louisiana State University, Baton Rouge, Louisiana 70803, USA*

and

K. T. HECHT †

*Department of Physics, University of Michigan, Ann Arbor, Michigan 48109, USA*

Received 2 February 1981

**Abstract:** A theoretical interpretation of the reduction in E2 strengths in $^{126}$Ba prior to backbending is presented. A shell model basis is built from normal parity orbitals organized into multiplets of a pseudo SU(3) symmetry coupled to $h_{11/2}$ configurations restricted to states of seniority zero and two. Within the framework of the model the scattering of a pair of protons from normal parity to the $h_{11/2}$ orbital produces band crossing and a corresponding reduction in E2 transition strengths prior to pair alignment which is the principal mechanism of the backbending.

## 1. Introduction

A recent report on transition strengths in $^{126}$Ba seems to indicate that E2 rates and backbending can be uncorrelated phenomena [1]). Experimental values for the $10^+ \rightarrow 8^+$ and $8^+ \rightarrow 6^+$ yrast transitions are less than one half those of an ideal rotor even though the onset of backbending is first seen at spin $10^+$. Band crossing and pair alignment models are predicated on backbending and a reduction in E2 rates being complementary phenomena. In the former case the yrast cascade is slowed by the shape change associated with backbending. In the latter case E2 rates are inhibited in the backbending region because the angular momentum of the core can undergo dramatic changes, by many units of $\hbar$, as the spins of a pair of particles in a large-$j$ orbital is aligned. Indeed earlier calculations for $^{126}$Ba [ref. [2,3])] and other studies [4,5]) for nuclei that display the backbending phenomenon predict a reduction in E2 strengths which is limited to levels lying in the backward sloping portion of the backbending yrast curve. It is thus not clear what mechanism can account for the observed pre-backbending reduction of E2 strengths in $^{126}$Ba.

In attempting to provide a microscopic shell-model interpretation of high-spin

† Supported in part by the US National Science Foundation.
†† Present address: National Chiao-Tung University, Hsin Chu, Taiwan, Republic of China.

phenomena we proposed a model based on the weak coupling of normal (N) parity orbitals comprised of all but the largest $j$-member of an oscillator shell and the unique or abnormal (A) parity level of largest $j$ from the next higher shell [6]). For $^{126}$Ba this means configurations of the type $(g_{\frac{7}{2}}, d_{\frac{5}{2}}, d_{\frac{3}{2}}, s_{\frac{1}{2}})^{n_N} \times (h_{11/2})^{n_A}$, where $n = n_N + n_A = 26$ is the number of spectroscopically active nucleons. A saving occurs when a restriction on the occupancies of the normal ($n_N$) and abnormal ($n_A$) parity orbitals can be justified. For deformed nuclei this is immediate. The deformation splits the $2j+1$ levels of each $j$-orbital into $j+\frac{1}{2}$ doublets. For any deformation the expected dominant configuration can then be determined by the pair-wise filling of the energetically favored or lowest Nilsson levels. As shown in fig. 1, for $^{126}$Ba with a deformation of 0.2 one expects the dominant configuration to have $n_N = 18$ and $n_A = 8$. Even so, matrix dimensionalities are enormous; for example, $(g_{\frac{7}{2}}, d_{\frac{5}{2}}, d_{\frac{3}{2}}, s_{\frac{1}{2}})^{n_N = 18, T_N = 4, J_N = 2}$ alone has a dimension of 5.372.930. Other restrictions are necessary if shell-model calculations are to be feasible.

Without the largest $j$-member of a shell the underlying oscillator structure is lost. But this seemingly unfavorable situation converts to a potentially favorable one upon recognizing that the remaining orbitals can be mapped onto a shell of one less pseudo-oscillator quantum [7]). For the Ba region this correspondence is $(g_{\frac{7}{2}}, d_{\frac{5}{2}}, d_{\frac{3}{2}}, s_{\frac{1}{2}}) \rightarrow (\tilde{f}_{\frac{7}{2}}, \tilde{f}_{\frac{5}{2}}, \tilde{p}_{\frac{3}{2}}, \tilde{p}_{\frac{1}{2}})$ where a tilde is used to denote pseudo-shell labels and $\boldsymbol{l}+\boldsymbol{s} = \boldsymbol{j} = \tilde{\boldsymbol{l}}+\tilde{\boldsymbol{s}}$. An advantage is gained by such a mapping if the physical hamiltonian is dominated by an invariant of a symmetry group that is inherent to the structure of the basis. The basis can then be truncated to the energetically favored representations of that group.

In the mapping from real to pseudo orbitals one must fix the relative phases of all orbitals [8]). It is essential to make that choice which maximizes the goodness of

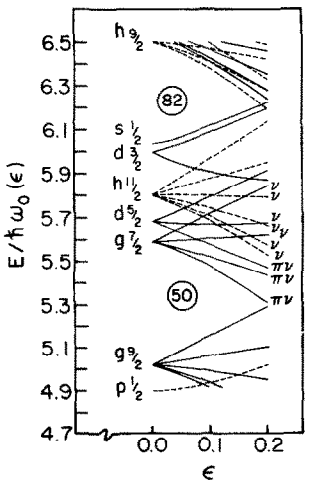


Fig. 1. Nilsson level scheme for nuclei with neutron and proton numbers between 50 and 82. The symbols $\nu$ and $\pi$ indicate filled neutron and proton orbitals of the $^{126}_{56}Ba_{70}$ ground-state configuration.

the underlying symmetry. Statistical spectroscopy provides an easy-to-apply method for doing this [9]). The correlation coefficient, $\zeta(-1 \leqq \zeta \leqq 1)$, between operators provides a measurement of the sameness of the two; i.e. how the expectation values of one vary as a function of the eigenvalues of the other. The optimum choice for relative phases is the one which maximizes the correlation between the physical hamiltonian and the second-order invariant of the symmetry group. For example, in mapping the upper fp shell onto a pseudo ds shell there are four distinct phase choices, $(f_{\frac{7}{2}}, p_{\frac{3}{2}}, p_{\frac{1}{2}}) \rightarrow (\tilde{d}_{\frac{5}{2}}, \pm\tilde{d}_{\frac{3}{2}}, \pm\tilde{s}_{\frac{1}{2}})$. With a choice for $H$ given by the effective interaction of Koops and Glaudemans [10]), the scalar correlation with $\tilde{Q}\cdot\tilde{Q}$ for a twelve-particle system ranges from a high of 0.59 for the optimum choice $(+, -, +)$ to a low of 0.15 $(+, +, -)$. In the ds shell where SU(3) is known to be good the twelve particle correlation coefficient between the interaction of Kuo [11]) and $Q\cdot Q$ is 0.56. For the upper fp shell one therefore expects the pseudo symmetry to be a useful scheme for basis truncation. The optimum choice for relative phases was fixed in this way for the mapping of the upper gds shell onto the $\tilde{\text{fp}}$ shell. A modified surface-delta interaction was chosen for $H$ since this is known to be a reasonable effective interaction for calculations in highly truncated model spaces [12]).

In our earlier publication we reported on a calculation for $^{126}$Ba in which the normal parity part of the space was truncated to the dominant U(10) symmetry and leading SU(3) symmetry of $(\tilde{\text{fp}})^{18}$, $[\tilde{f}] = [444222]$ and $(\tilde{\lambda}\tilde{\mu}) = (24, 0)$. For the abnormal parity space a basis was formed from the seniority zero and two states of $(h_{11/2})^8$ $T = 4$. Strengths of the SDI interaction in the N and A spaces were taken to be free parameters as was the strength of the multipole-multipole interaction, also taken to be of SDI form, coupling the two. Single-particle energies were fixed to produce a 2.5 MeV separation of the $\tilde{l} = 1$ and $\tilde{l} = 3$ centroids. As the basis was restricted to $\tilde{S} = 0$ states, matrix elements of $\tilde{l}\cdot\tilde{s}$, which are normally used to effect a splitting of the $j = \tilde{l} \pm \frac{1}{2}$ orbitals, vanished and were not included. Backbending was found to be a pair alignment phenomenon. For $E \lesssim \Delta$, where $\Delta$ is the energy separation between the $0^+$ state and the centroid of the $v = 2$ states of the $h_{11/2}$ configuration, the yrast states are formed by coupling the $v = 0$ state to the first few excitations of the N-space. For $E > \Delta$, it is the coupling of $v = 2$ states to the lowest spin states of the N-space that dominates the structure of the yrast band.

## 2. The model

### 2.1. BASIS STATES

A complete labelling of the weak coupled basis states, with the relevant group structure noted below, is

$$|[l^{n_N}]\ [\tilde{f}]\ \tilde{\alpha}(\tilde{\lambda}\ \tilde{\mu})\tilde{K}\ \tilde{L}\ \tilde{\beta}(\tilde{S}\quad T_N\ )J_N;(h_{11/2})^{n_A}(\ v\ t)\beta T_A J_A:\ T\quad J\ \rangle. \tag{1}$$

$$\begin{array}{llllllllllll} | & | & | & | & & | & & | & | & & | & | \\ \text{U(40)} & \text{U(10)} & \text{SU(3)} & & \text{R(3)} & & & & \text{U(12)} & \text{R(5)} & & \text{SU(2)}_T \\ & & & & & \text{SU(2)}_{\tilde{S}}\times\text{SU(2)}_T & & & & & & & \text{SU(2)}_J \end{array}$$

The U(40) → U(10) × U(4) reduction partitions the normal parity part of the space into its space and pseudospin-isospin parts. A running index $\tilde{\alpha}$ is used to distinguish multiple occurrences of a given pseudo SU(3) symmetry $(\tilde{\lambda}\tilde{\mu})$ in a particular U(10) symmetry, $[\tilde{f}]$, of the $(\tilde{\mathrm{fp}})$ shell. Similarly $\tilde{\beta}$ is a running index used whenever necessary to distinguish multiple occurrences of $(\tilde{S}T)$ pairs in a U(4) symmetry. This supermultiplet symmetry need not be specified for it must be conjugate to the U(10) symmetry for the basis states to be properly antisymmetrized. The U(12) → R(5) reduction organizes the abnormal parity part of the basis into quasispin multiplets carrying seniority and reduced isospin labels $(v, t)$, respectively. The index $\beta$ is used to resolve isospin multiplicities. A more detailed explanation of the normal parity state labels can be found in ref. [7]) while a discussion of the quasispin geometry can be found in ref. [13]).

Our previous calculation did not include the possibility of scattering particles between normal and abnormal parity orbitals. For $^{126}$Ba the most important of these are $n_{\mathrm{N}} = 18 \pm 2$, $n_{\mathrm{A}} = 8 \mp 2$. Single-particle excitations are excluded for they connect to states of opposite parity. Of the pair scattering configurations that can couple to the dominant configuration,

$$[(\tilde{\mathrm{fp}})^{18}[444222](\tilde{\lambda}\tilde{\mu}) = (24, 0)T_{\mathrm{N}} = 3; (\mathrm{h}_{\frac{11}{2}})^{8}T_{\mathrm{A}} = 4]T = 7, \tag{2a}$$

the following two should be the most important:

$$[(\tilde{\mathrm{fp}})^{16}[44422](\tilde{\lambda}\tilde{\mu}) = (22,4)T_{\mathrm{N}} = 2; (\mathrm{h}_{\frac{11}{2}})^{10}T_{\mathrm{A}} = 5]T = 7,$$
$$[(\tilde{\mathrm{fp}})^{16}[442222](\tilde{\lambda}\tilde{\mu}) = (20,2)T_{\mathrm{N}} = 4; (\mathrm{h}_{\frac{11}{2}})^{10}T_{\mathrm{A}} = 3]T = 7. \tag{2b}$$

The first of these perturbing configurations corresponds to a pair of neutrons ($\nu$) and the second to a pair of protons ($\pi$) being lifted to the $\mathrm{h}_{\frac{11}{2}}$ orbital. Including all three but restricting the $\mathrm{h}_{\frac{11}{2}}$ space to $v = 0$ and $v = 2$ states with $t = 1$, yields for $J = 0, 2, 4, \ldots, 16$ a basis of size 53, 193, 312, 402, 462, 494, 503, 492, 466, respectively. (In the $\pi$-scattering case $v = 2$, $t = 0$ states exist but only for $T_{\mathrm{A}} = 4$. Such states are expected on the average to lie at an energy of about 5 MeV above the $T_{\mathrm{A}} = 3$, $t = 1$ states, and they have therefore been excluded. The $v = 2$, $t = 1$ $\pi$-scattering states occur with multiplicity two). Though these dimensionalities are manageable, we have chosen to separate the problem into two parts, one of which includes only the possibility of neutron pair scattering and excludes the $K = 4$ band of the (22, 4) representation, labelled model II($\nu$) in what follows. A second labelled model II($\pi$), includes only the leading proton scattering configuration. Model I will be used to reference results which do not include pair scattering basis states. Models I, II($\nu$) and II($\pi$) have dimensionalities: (6, 27, 27), (16, 91, 94), (24, 146, 150), (30, 188, 192), (34, 216, 220), (36, 232, 234), (36, 238, 236), (36, 239, 228), (35, 238, 213) for $J = 0, 2, 4, \ldots, 16$, respectively.

## 2.2. TENSOR INTERACTION

The hamiltonian has the general form

$$H = C_{\tilde{l}^2} \sum_{\alpha}^{n^N} \tilde{l}_{\alpha}^2 + C_{\tilde{l}\cdot\tilde{s}} \sum_{\alpha}^{n^N} \tilde{l}_{\alpha} \cdot \tilde{s}_{\alpha} + \varepsilon_A n_A + G_N H_N + G_A H_A + G_M H_M + G_P H_P. \quad (3)$$

The first three terms are one-body potentials which generate, respectively, the separation of the $\tilde{l} = 1, 3$ centroids, the $j = \tilde{l} \pm \frac{1}{2}$ splitting, and the placement of the abnormal parity level relative to the normal parity ones. In the restricted basis of our models $\tilde{S}_N = 0$ so contributions from the $\tilde{l} \cdot \tilde{s}$ term vanish. We choose $C_{\tilde{l}^2} = 0.225$ MeV. Apart from an additive constant this corresponds to single-particle energies $\varepsilon_{\frac{1}{2}} = \varepsilon_{\frac{3}{2}} = -2.02$ MeV and $\varepsilon_{\frac{5}{2}} = \varepsilon_{\frac{7}{2}} = -4.27$ MeV. The single-particle energy of the abnormal parity level is only important when the model space includes pair scattering configurations. For $^{126}$Ba model II studies we set $\varepsilon_{h_{\frac{11}{2}}} = -2.10$ MeV. These values are compatible with single-particle systematics in the region [14]).

The last four terms in eq. (3) are two-body interactions. The form for these was chosen to be a surface-delta interaction. The labels N and A refer to the normal and abnormal parity spaces while $H_M$ and $H_P$ are multipole-multipole and pair scattering terms which couple the two. The strength factors were taken to be independent parameters. The values used in the present study are given in table 1. The pair scattering interaction is only effective for model II studies.

TABLE 1

Strength parameters of the surface-delta interaction

| Model | Strength parameters | | | |
|---|---|---|---|---|
| | $G_N$ | $G_A$ | $G_M$ | $G_P$ |
| I | 0.26 | 0.61 | 0.12 | |
| II($\nu$) | 0.24 | 0.62 | 0.12 | 0.20 |
| II($\pi$) | 0.30 | 0.58 | 0.12 | 0.10 |

Numbers quoted are all relative to unity which produces 6 MeV binding for the $(h_{11/2})^2$ $(v, J) = (0, 0)$ configuration.

## 2.3. MATRIX ELEMENTS

The procedure for evaluating matrix elements is straightforward. First both interaction and excitation operators are written in second quantized form. It is important to emphasize that real matrix elements are input at this stage of the calculation. For example, the input SDI matrix elements of the present study are for the real $g_{\frac{7}{2}}$, $d_{\frac{5}{2}}$, $d_{\frac{3}{2}}$, $s_{\frac{1}{2}}$ orbitals. This second quantized form for the operator is then transformed into its pseudo space analog. Group coupling and recoupling

techniques are then used to express the latter in terms of standard tensor operators [15]). Examples for the $\tilde{l}^2$ and $\tilde{l} \cdot \tilde{s}$ terms of $H$ are given in ref. [7]). See also ref. [16]), and for the tensor decomposition of the E2 operator, ref. [17]). Matrix elements of the tensors can be evaluated using the coefficient of fractional parentage and reduced matrix element programs of Braunschweig [18]) together with SU(3) and SU(2) coupling and recoupling routines [19]). Hemenger and Hecht give analytic results for A-space matrix elements [13]). We leave to a future paper a more detailed discussion of these matters.

## 3. Results for $^{126}$Ba

Two basic phenomena appear to play a role in the backbending region of the $^{126}$Ba yrast curve; (a) band crossing involving different pseudo SU(3) representations of the normal parity part of the basis, and (b) pair alignment in which a pair of nucleons from the high-$j$ abnormal parity orbital align their spins to maximum possible $J$. It is advantageous to examine these phenomena separately.

### 3.1. N-SPACE BAND CROSSING

Energy spectra from diagonalizations of our effective interaction, eq. (3) with two-body parts of SDI form and strengths given in table 1, are shown in fig. 2. This figure shows the spectra of pure normal parity configurations. $(\tilde{fp})^{n_N}$ coupled to $v = 0, J_A = 0$ states of $(h_{\frac{11}{2}})^{n_A}$ both for the separate pseudo SU(3) representations used in the present study, (with the pair-scattering term, $H_P$ "turned off"), and for the mixed pseudo SU(3) representations, (with $H_P$ "turned on"). The effective moment of inertia of the (24, 0) representation is almost identical to that of the $K = 0$ band of the (22, 4) $\nu$-scattering representation but less than the moment of inertia of the $K = 0$ band of the (20, 2) $\pi$-scattering representation. In the (24, 0)+(20, 2) calculation the (24, 0) representation thus dominates for low-spin yrast states; but for higher spins, because of its larger moment of inertia and correspondingly compressed rotational spectrum, members of the (20, 2) $\pi$-scattering band are energetically favored. For $\varepsilon_{\frac{11}{2}} = -2.1$ MeV the transition occurs between spins 8–12 and accounts for the non-rotational character of the (24, 0)+(20, 2) results in that region. The (24, 0)+(22, 4) spectrum shows no such irregularity, all states of the yrast band are dominated by the (24, 0) representation. The effect of the (22, 4) representation is manifest in increased binding of the lower yrast states, hence an expanded spectrum for (24, 0)+(22, 4) compared to (24, 0), but no crossing of bands is found. The (24, 0)+(20, 2)+(22, 4) results are nearly indistinguishable, even in detail, from the (24, 0)+(20, 2) case.

The band-crossing phenomenon found in the (24, 0)+(20, 2) results is shown more clearly in fig. 3 where the excitation energies of the lowest two eigenstates for

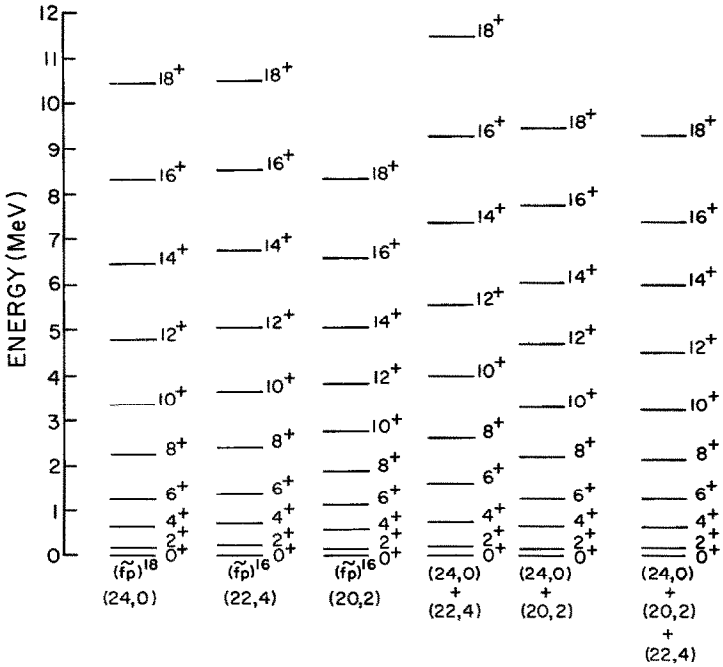


Fig. 2. Calculated spectra for $H$ diagonalized in leading pseudo SU(3) symmetries: $(\tilde{\lambda}\tilde{\mu}) = (24, 0)$ of $(\tilde{fp})^{18}$ coupled with the $v = 0$, $J_A = 0$ state of $(h_{11/2})^8$, and $(\tilde{\lambda}\tilde{\mu}) = (22, 4)$, $(20, 2)$ of $(\tilde{fp})^{16}$ coupled with the $v = 0$, $J_A = 0$ state of $(h_{11/2})^{10}$, and combinations of these configurations included in the present study. The moment of inertia of the (20, 2) representation is greater than that of the (24, 0) and (22, 4) representation. This leads to band crossing in the (24, 0)+(20, 2) mixing results, the signature of which is spectrum compression between spins 8 and 14.

each spin are plotted versus $I(I+1)$. The [(24, 0)/(20, 2)] mixing percentages for the yrast states change from $(\frac{98}{2}) \rightarrow (\frac{96}{4}) \rightarrow (\frac{80}{20}) \rightarrow (\frac{6}{94}) \rightarrow (\frac{2}{98})$ for $J = 6 \rightarrow 14$, respectively. The effect of the band mixing can also be seen on a $\Delta E$ versus $I$ plot, fig. 4. For an ideal rotor one expects a straight line with slope proportional to the inverse of the moment of inertia. The (24, 0) result is of that type but for (24, 0)+(20, 2) there is a smooth transition from the (24, 0) to the (20, 2) rotor values. Also shown are model I, II($\pi$) and experimental results. We will return to these later. Though band crossing introduces a phase transition, it alone does not reproduce experimental findings.

### 3.2. A-SPACE PAIR ALIGNMENT

The eigenvalue spectrum from a diagonalization of $H$ in the pure abnormal parity configuration $(h_{\frac{11}{2}})^8$ $T = 4$, restricted to seniority zero and two, is shown in fig. 5. The $(h_{\frac{11}{2}})^{10} T = 5$ and $(h_{\frac{11}{2}})^{10}$ $T = 3$ spectra are similar though for the latter each $J_A(v = 2, t = 1)$ state occurs twice. The N-space I, II($v$), II($\pi$) results shown are, respectively, a repeat of the (24, 0) and (24, 0)+(22, 4) and (24, 0)+(20, 2)

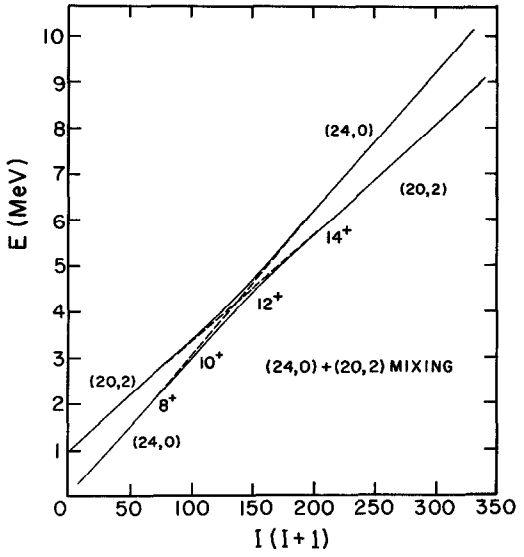


Fig. 3. Band crossing in the normal parity part of the model II ($\pi$) space. The (24, 0)/(20, 2) mixing ratios for spins 8–14 are 96/4, 80/20, 6/94, 2/98, respectively.

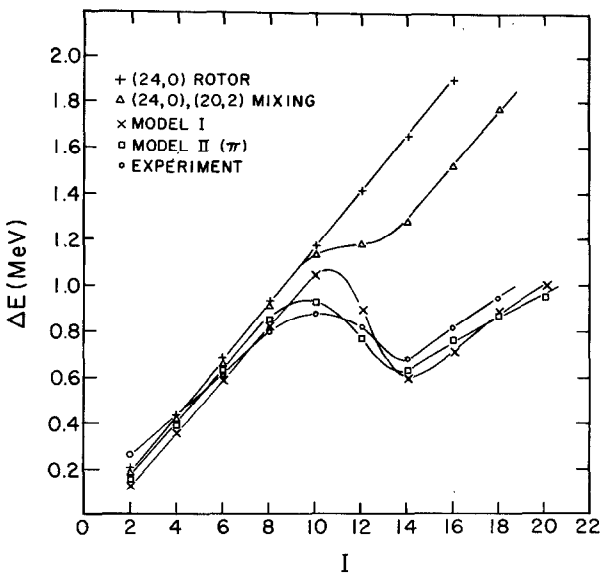


Fig. 4. $\Delta E$ versus $I$ plots. A departure from linearity signals non-rotational behavior. The mixing transition is due to band crossing. The abruptness of the pair alignment transition for model I is smoothed by prealignment band mixing in model II($\pi$). Experimental results are from ref. [20]).

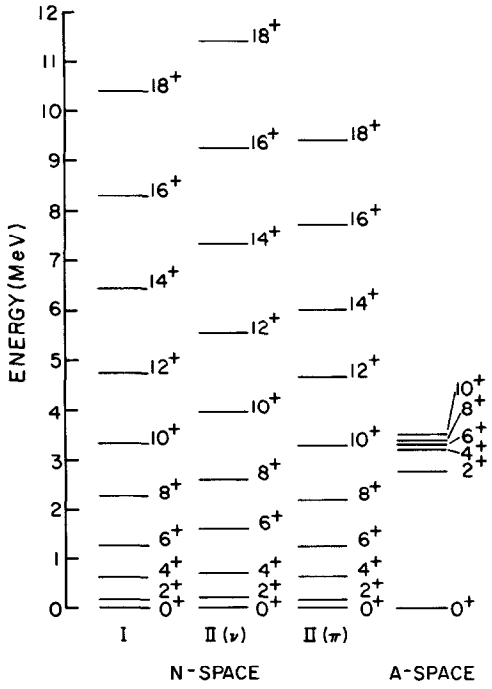


Fig. 5. Energy spectra from diagonalizations of a surface delta interaction in the normal and abnormal parity parts of model spaces for $^{126}$Ba. Model I refers to the $(\tilde{\lambda}\tilde{\mu}) = (24, 0)$ subspace of the $(\tilde{fp})^{18}$ $T = 3$ configuration. Model II($\nu$) and II($\pi$) include in addition (22, 4) and (20, 2) neutron and proton scattering representations, respectivly. Band crossing accounts for the compression of the II($\pi$) spectrum between spins 8–16.

spectra given in fig. 2. Comparing the N and A space spectra one can see immediately that a weak coupling of the two leads to a pair alignment phenomenon. For an excitation energy less than about 3 MeV, $I \lesssim 8$, the yrast states can be built most economically by coupling the fully paired $J_A = 0$ configuration of the A-space to the N-space core. For an excitation energy greater than 3 MeV, $I \gtrsim 10$, it is the coupling of unpaired ($J_A \neq 0$) configurations to states of low N-space excitation (with small $J_N$ values) that is energetically favored. Thus, while for $I = 8$ ($J_N = 8$) $\times$ ($J_A = 0$) dominates, for $I = 12$ it is ($J_N = 2$) $\times$ ($J_A = 10$) that is the predicted dominant structure. Between spins 8 and 12 rotational alignment occurs; that is, one moves from a situation where the projection of $\boldsymbol{J}_A$ onto a unit vector in the $\boldsymbol{I}$ direction is zero to one where the value of that projection is its maximum. The probability of finding $J_A \neq 0$ configurations in the yrast states of spin $I$ is plotted versus $I$ in fig. 6. Note that the transition is much sharper for Model I and II($\nu$) than for II($\pi$). This is due to configuration mixing. Note that the $[(20,2)J_N = 8] \times [J_A = 2]$ coupling makes a significant contribution to the model II($\pi$) $I = 10$

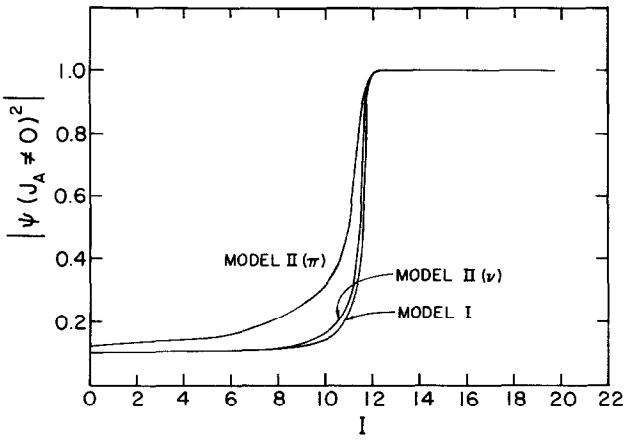


Fig. 6. Probability of finding pairs in the abnormal parity space coupled to non-zero angular momentum.

yrast state, see table 2. The amount of mixing depends of course upon the strenghts of the N-A space interaction terms $H_M$ and $H_P$.

### 3.3. BACKBENDING AND THE $B$(E2) ANOMALY

The "backbending" is most apparent when the inertial constant,

$$2\mathcal{I}/\hbar^2 \equiv (4I-2)/\Delta E_\gamma, \tag{4a}$$

of the yrast states is plotted as a function of the square of the rotational frequency,

$$(\hbar\omega)^2 \equiv \Delta E_\gamma^2/\{[I(I+1)]^{\frac{1}{2}}-[(I-2)(I-1)]^{\frac{1}{2}}\}^2. \tag{4b}$$

Backbending curves for $^{126}$Ba are shown in fig. 7. Experimental results are from the work of Flaum *et al.* [20]). For a rigid rotor, one expects a horizontal line. For $I \leqq 8$ all three models yield such a result. The $(\tilde{\lambda}\tilde{\mu})$ mixing in model II($\nu$) and especially in model II($\pi$) softens the core somewhat bringing the $\mathcal{I}$ versus $\omega^2$ curves in closer agreement with experiment. The interaction parameters, table 1, were adjusted to reproduce the excitation energy of the $I^\pi = 8^+$ level, the onset of backbending at $I^\pi = 10^+$ and, as best possible short of a least squares analysis, the backsloping and upper branches of the experimental backbending curve. If the (24,0)+(20,2) N-space mixing result were superimposed on the $\mathcal{I}$ versus $\omega^2$ curves it would follow the model I results up to spin 10, rise slightly and then continue horizontally at the value of $\mathcal{I}(2\mathcal{I}/\hbar^2 \approx 45\ \text{MeV}^{-1})$ for the (20, 2) representation. The backward sloping character of the curve is not part of that picture. One can also see from the results for $\Delta E$ versus $I$ given in fig. 4 that alignment is the primary mechanism responsible for the backbending. Note that the prealignment band crossing smooths the $\Delta E$ versus $I$ transition bringing it also in close agreement with experiment.

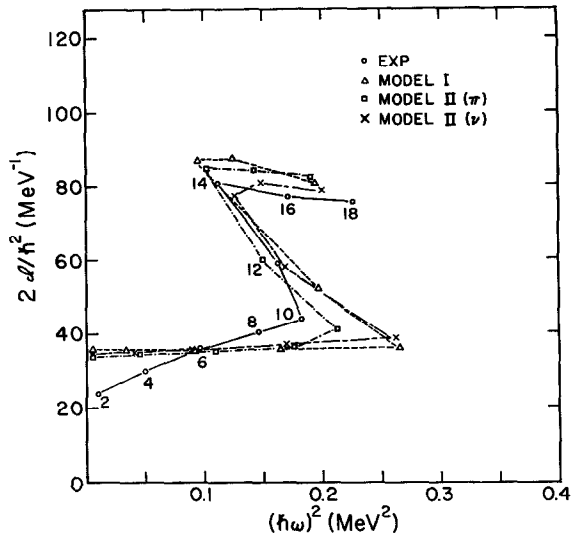


Fig. 7. Backbending in $^{126}$Ba. The curves were calculated using $2\mathscr{I}/\hbar^2 = (4I-2)/\Delta E$ and $(\hbar\omega)^2 = \Delta E^2/\{[I(I+1)]^{1/2}-[(I-2)(I-1)]^{1/2}\}^2$. Experimental results are from ref. [20]).

The effect of the band crossing on E2 rates is illustrated in fig. 8. The experimental results are from ref. [1]). Model I predictions are not shown for they follow rigid rotor values up through spin 10. As the E2 operator, approximately transformed into the pseudo scheme, is nearly a generator of the pseudo SU(3) symmetry, it at most only weakly couples different $(\tilde{\lambda}\tilde{\mu})$ representations. The prealignment fall off in E2 strengths found for model II ($\pi$) is due to $(\tilde{\lambda}\tilde{\mu})$ mixing. Amplitudes of the leading components in the model I and model II ($\pi$) yrast eigenstates are given in table 2. The (20, 2) representation makes a small but non-negligible contribution to the lowest model II($\pi$) eigenstates with $I \leqq 6$ and actually dominates for spins 8 and 10. The $8^+ \rightarrow 6^+$ transition strength is no smaller than it is because the (24, 0) $\rightarrow$ (24, 0) and (20, 2) $\rightarrow$ (20, 2) strengths, though separately less because of the reduced amplitude factors, add coherently.

Earlier calculations [2]) for the yrast transitions in $^{126}$Ba predict a significant (sharp) reduction in E2 strengths only for levels lying on the backward rising slope of the backbending curve. Calculations based on the interacting boson model [21]) show some decrease in E2 strengths with increasing angular momenta, but this decrease seems to arise from the natural differences between the SU(3) limit and rigid rotor models. The interacting boson-pair alignment model calculation of Gelberg and Zemel [3]) on the other hand predicts a reduction in E2 strength prior to the backbending very similar to ours and, although more phenomenological, does indeed contain some of the physics of our microscopic model. Although the E2 reduction factors predicted by our model II($\pi$) calculation are less or seem to lag those observed experimentally, we believe that the phenomenon of band crossing

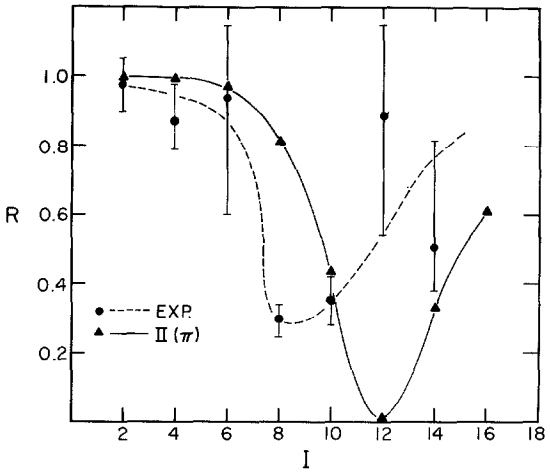


Fig. 8. Normalized $B$(E2) rates:

$$R = \left[\frac{B(\mathrm{E2}, I \to I-2)}{B(\mathrm{E2}, 2 \to 0)}\right] \Big/ \left[\frac{B(\mathrm{E2}, I \to I-2)}{B(\mathrm{E2}, 2 \to 0)}\right]_{\mathrm{rotor}}$$

Experimental results are from ref. [1]).

prior to pair alignment gives the mechanism which can account for the prealignment E2 anomaly. A more realistic quantitative prediction would undoubtedly require the use of a larger normal parity basis space. The need for representation mixing is also evident from the fact that the calculated spectra are too rigid as indicated by the nearly horizontal slope of the $\mathscr{I}$ versus $\omega^2$ curve in the $I^\pi = 2^+ \to 10^+$ region (fig. 7).

A typical model II($\pi$) spectrum for $^{126}$Ba is shown in fig. 9 alongside the experimental level scheme. We have found that details concerning E2 branching to and/or from yrast states in the backbending region are sensitive to model parameters. Experimentally there are two nearly degenerate $12^+$ states and the model II($\pi$) spectrum agrees with this. However, whereas the experimental $12_1^+ \to 10_1^+$ strength is large, our model II($\pi$) study yields a weak $12_1^+ \to 10_1^+$ transition but a strong $12_2^+ \to 10_1^+$ E2 coupling. One refinement is to adjust the $h_{\frac{11}{2}}$ single-particle energy to gain a mixing of the $12_1^+$ state of mainly (24, 0) $J_N = 2$, $J_A = 10$ character with the $12_2^+$ state of mainly (20, 2)$J_N = 2$, $J_A = 10$ character. This has been tried with positive results, but in so doing the $\mathscr{I}$ versus $\omega^2$ curve, which we find to be very sensitive to even small changes in the structure of the eigenstates, is made less good. The use of a larger basis could conceivably resolve the discrepancy also.

TABLE 2

Main components of the calculated yrast eigenstates for models I and II($\pi$)

| State | Model I | Model II($\pi$) |
|---|---|---|
| $0^+$ | (0.95) $\|(24, 0)J_N = 0, (h_{11/2})^8 J_A = 0\rangle$ | (0.91) $\|(24, 0)J_N = 0, (h_{11/2})^8 J_A = 0\rangle$<br>+(0.24) $\|(20, 2)J_N = 0, (h_{11/2})^{10} J_A = 0\rangle$ |
| $2^+$ | (0.95) $\|(24, 0)J_N = 2, (h_{11/2})^8 J_A = 0\rangle$ | (0.91) $\|(24, 0)J_N = 2, (h_{11/2})^8 J_A = 0\rangle$<br>+(0.24) $\|(20, 2)J_N = 2, (h_{11/2})^{10} J_A = 0\rangle$ |
| $4^+$ | (0.95) $\|(24, 0)J_N = 4, (h_{11/2})^8 J_A = 0\rangle$ | (0.90) $\|(24, 0)J_N = 4, (h_{11/2})^8 J_A = 0\rangle$<br>+(0.25) $\|(20, 2)J_N = 4, (h_{11/2})^{10} J_A = 0\rangle$ |
| $6^+$ | (0.94) $\|(24, 0)J_N = 6, (h_{11/2})^8 J_A = 0\rangle$ | (0.86) $\|(24, 0)J_N = 6, (h_{11/2})^8 J_A = 0\rangle$<br>+(0.35) $\|(20, 2)J_N = 6, (h_{11/2})^{10} J_A = 0\rangle$ |
| $8^+$ | (0.94) $\|(24, 0)J_N = 8, (h_{11/2})^8 J_A = 0\rangle$ | (0.44) $\|(24, 0)J_N = 8, (h_{11/2})^8 J_A = 0\rangle$<br>+(0.76) $\|(20, 2)J_N = 8, (h_{11/2})^{10} J_A = 0\rangle$ |
| $10^+$ | (0.93) $\|(24, 0)J_N = 10, (h_{11/2})^8 J_A = 0\rangle$ | (0.14) $\|(24, 0)J_N = 10, (h_{11/2})^8 J_A = 0\rangle$<br>+(0.83) $\|(20, 2)J_N = 10, (h_{11/2})^{10} J_A = 0\rangle$<br>+(0.32) $\|(20, 2)J_N = 8, (h_{11/2})^{10} J_A = 2\rangle$ |
| $12^+$ | (0.60) $\|(24, 0)J_N = 2, (h_{11/2})^8 J_A = 10\rangle$<br>+(0.73) $\|(24, 0)J_N = 4, (h_{11/2})^8 J_A = 10\rangle$ | (0.65) $\|(24, 0)J_N = 2, (h_{11/2})^8 J_A = 10\rangle$<br>+(0.69) $\|(24, 0)J_N = 4, (h_{11/2})^8 J_A = 10\rangle$ |
| $14^+$ | (0.81) $\|(24, 0)J_N = 4, (h_{11/2})^8 J_A = 10\rangle$<br>+(0.51) $\|(24, 0)J_N = 6, (h_{11/2})^8 J_A = 10\rangle$ | (0.85) $\|(24, 0)J_N = 4, (h_{11/2})^8 J_A = 10\rangle$<br>+(0.42) $\|(24, 0)J_N = 6, (h_{11/2})^8 J_A = 10\rangle$<br>+(0.19) $\|(20, 2)J_N = 4, (h_{11/2})^{10} J_A = 10\rangle$ |

The $(24, 0) \leftrightarrow (20, 2)$ band crossing between spins 6 and 10 results in reduced $B$(E2) strengths prior to the pair alignment transition which occurs between spins 10 and 12.

## 4. Concluding remarks

The observed prealignment reduction in $B$(E2) rates in $^{126}$Ba poses an interesting theoretical challenge, for neither band crossing or pair alignment models offer a simple explanation. We have shown that a weak coupling model based on normal parity configurations organized into multiplets of pseudo SU(3) symmetry and abnormal parity configurations organized in multiplets of R(5) quasispin symmetry offers a satisfactory framework for studying backbending and related phenomena. Pair alignment emerges as the primary mechanism of backbending but band crossing can be competitive and when it is, anomalous E2 behavior can be expected.

Though fully microscopic, our weak coupling picture is schematic. The truncation

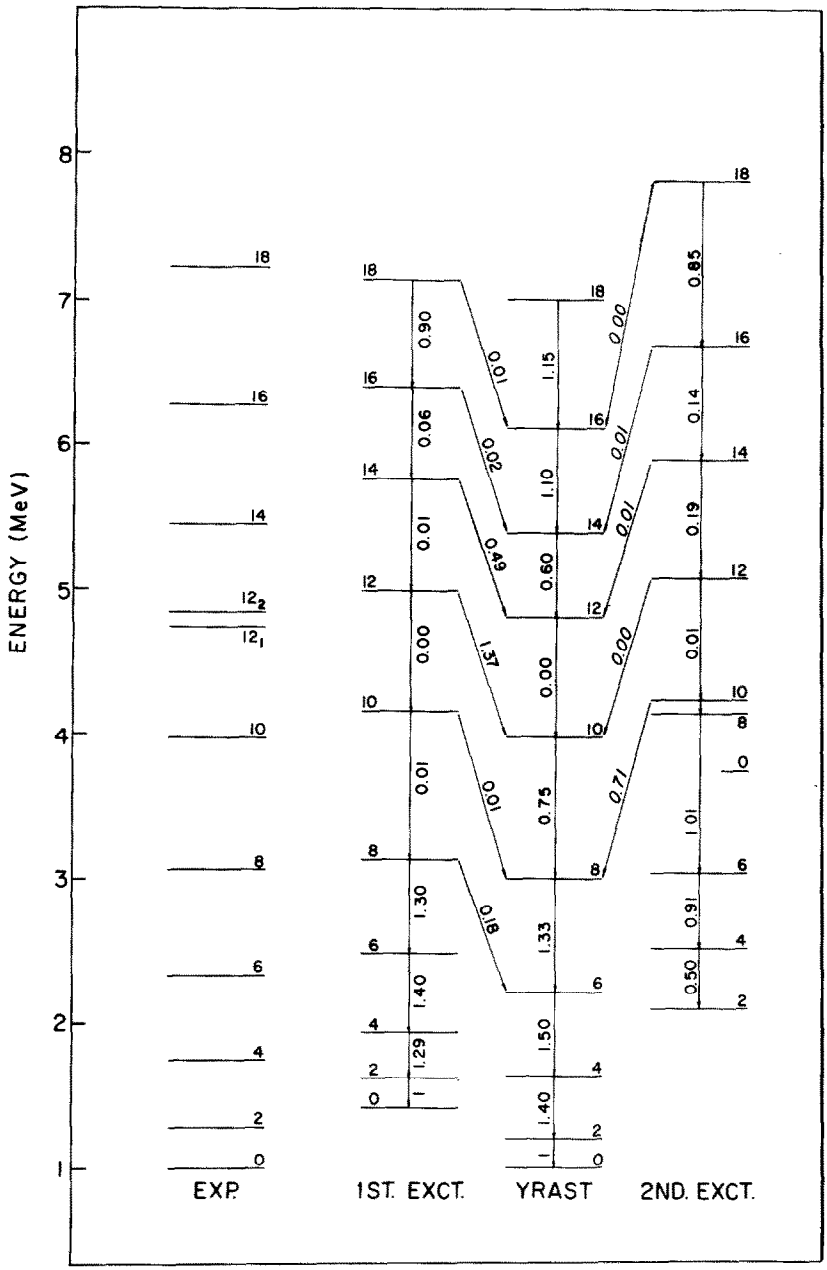


Fig. 9. Energy spectra for $^{126}_{56}Ba_{70}$. Experimental results are from ref. [20]). Calculated numbers are for model II($\pi$). E2 strengths are for proton and neutron effective charges $e_\pi = (1+0.5)e$ and $e_\nu = 0.5e$. Numbers quoted are relative to the $2^+ \rightarrow 0^+$ transition for which the strength is $0.21 \times 10^{-48} e^2 \cdot \mathrm{cm}^4$.

employed is severe. For this reason we do not claim high accuracy nor do we expect detailed agreement between theory and experiment. Nonetheless, we do believe the essential physics has been bared. We look forward to applications in the Ge region where forking to non-yrast states in the backbending region has been observed [22]. For this it is the coupling of a pseudo ds shell with $g_{\frac{9}{2}}$ configurations that enter.

One of the authors (K.T.H.) gratefully acknowledges the support of the Alexander von Humboldt Foundation through a US Senior Science fellowship, the hospitality of the Max-Planck-Institut für Kernphysik, Heidelberg, and the stimulus of the experimental work of the Heidelberg group.

## References

1) G. Seiler-Clark, D. Husar, R. Novotny, H.Gräf and D. Pelte, Phys. Lett. **80B** (1979) 345
2) M. Reinecke and H. Ruder, Z. Phys. **A282** (1976) 400; private communication quoted in ref. 1)
3) A. Gelberg and A. Zemel, Phys. Rev. **C22** (1980) 937
4) F. Grümmer, K. W. Schmid and A. Faessler, Nucl. Phys. **A317** (1979) 287
5) C. Roulet, H. Sergolle, P. Hubert, T. Linblad, E. Grosse, D. Schwalm, D. Fuchs, H. Wallersheim, J. Idzko and H. Emling, to be published
6) R. D. Ratna Raju, K. T. Hecht, B. D. Chang and J. P. Draayer, Phys. Rev. **C20** (1979) 2397
7) R. D. Ratna Raju, J. P. Draayer and K. T. Hecht, Nucl. Phys. **A202** (1973) 433
8) T. Inoue, Y. Akiyama and K. Shirai, Proc. Inst. Natural Sciences, Nihon Univ. **12** (1977) 15
9) J. B. French, Phys. Lett. **26B** (1967) 75;
T. R. Halemane, K. Kar and J. P. Draayer, Nucl. Phys. **A311** (1978) 301
10) J. E. Koops and P. W. M. Glaudemans, Z. Phys. **A280** (1977) 181
11) T. T. S. Kuo, Nucl. Phys. **A103** (1967) 71
12) J. P. Schiffer, in Two-body force in nuclei, ed. S. M. Austin and G. M. Crawley (Plenum, New York, 1972)
13) K. T. Hecht, Nucl. Phys. **A102** (1967) 11;
R. P. Hemenger and K. T. Hecht, Nucl. Phys. **A145** (1970) 468 [Note on erratum in ref. [6])]
14) A. L. Goodman, Nucl. Phys. **A331** (1979) 401
15) K. T. Hecht, in Ann. Rev. Nucl. Sci., Vol. 23, ed. E. Segre (Annual Reviews, Palo Alto, California, 1973)
16) J. P. Draayer, Nucl. Phys. **A216** (1973) 457
17) D. Braunschweig and K. T. Hecht, Phys. Lett. **77B** (1978) 33
18) D. Braunschweig, Comp. Phys. Com. **14** (1978) 109; **15** (1978) 259
19) Y. Akiyama and J. P. Draayer, Comp. Phys. Comm. **5** (1973) 405
20) C. Flaum, D. Cline, A. W. Sunyar, O. C. Kistrer, Y. K. Lee and J. S. Kim, Nucl. Phys. **A264** (1976) 291
21) H. Emling, in Interacting bosons in nuclear physics, ed. F. Iachello (Plenum, New York, 1979)
22) A. P. deLima, J. H. Hamilton, A. V. Ramayya, B. van Nooijen, R. M. Ronningen, H. Kawakami, R. B. Piercey, E. deLima, R. L. Robinson, H. J. Kim, W. K. Tuttle, L. K. Peker, F. A. Richey and R. Popli, Phys. Lett. **83B** (1979) 43